International Journal of Biochemistry and Cell Biology 113 (2019) 104–114

Contents lists available at ScienceDirect

International Journal of Biochemistry and Cell Biology

journal homepage: www.elsevier.com/locate/biocel

Sinoporphyrin sodium based sonodynamic therapy induces anti-tumor effects in hepatocellular carcinoma and activates p53/caspase 3 axis

Enze Li[a,b,1], Yi Sun[c,1], Guixiang Lv[d], Yongning Li[b], Zhiguo Zhang[e], Zheng Hu[b,*], Wenwu Cao[b,f,*]

[a] School of Life Science and Technology, Harbin Institute of Technology, Harbin, China
[b] Laboratory of Sono- and Photo-theranostic Technologies, Harbin Institute of Technology, Harbin, China
[c] Department of Stomatology, The Fourth Affiliated Hospital, Harbin Medical University, Harbin, China
[d] Department of Biochemistry and Molecular Biology, Harbin Medical University, Harbin, China
[e] Condensed Matter Science and Technology Institute, Harbin Institute of Technology, Harbin, China
[f] Department of Mathematics and Materials Research Institute, The Pennsylvania State University, University Park, Pennsylvania, USA

ARTICLE INFO

Keywords:
Sinoporphyrin sodium
Sonodynamic therapy
Hepatocellular carcinoma
Reactive oxygen species
Apptosis

ABSTRACT

Sonodynamic therapy (SDT) is a noninvasive therapeutic method via the activation of certain chemical sensitizers using low intensity ultrasound. In this work, we evaluated the antitumor effect of sinoporphyrin sodium (DVDMS) mediated SDT (DVDMS-SDT) on Hepatocellular carcinoma (HCC) cell lines both in vitro and in vivo. The results indicated that DVDMS-SDT was significantly more efficacious than PpIX-SDT in treating hepatocellular cell line Hep-G2. DVDMS-SDT also increased the ratio of cells in the G2/M phase and decreased the CDK1 and Cyclin B1 protein level. DVDMS-SDT markedly increased intracellular reactive oxygen species (ROS) *in vitro*. The increased ROS production up-regulated the expression of p53 and Bax, and down-regulated Bcl-2 expression, which led to the activation of caspase-3, ultimately initiated cell apoptosis. These effects could be partially reversed by the ROS scavenger N-acetylcysteine (NAC). *In vivo* experiments revealed that the DVDMS-SDT resulted in an effective inhibition of tumor growth and prolonged the survival time of tumor-bearing mice. More importantly, no obvious signs of side effects were observed. These results suggested that DVDMS-SDT is very effective in treating Hepatocellular carcinoma without side effects. The primary mechanism of SDT is due to the increased ROS activated the p53/Caspase 3 axis of apoptosis.

1. Introduction

Hepatocellular carcinoma (HCC) is considered one of the most globally widespread malignancies and the third leading cause of tumor mortality (Torre et al., 2012). Current treatments for HCC include surgery, radiation therapy and chemotherapy, but these methods have their own limitations. HCC is particularly insensitive to chemotherapy. Surgery is the conventional approach to treat HCC, but only 1/3 of cases are identified at early stages and treatable by surgery due to the high invasiveness and fast development of HCC (Li et al., 2016; Ma et al., 2017). The resection rate for HCC is less than 15%, while the postoperative recurrence rate is approximately 50% (Roayaie et al., 2015; Bruix et al., 2015). These existing problems demand the search for new therapeutic methods for more successful intervention.

Sonodynamic therapy (SDT) was initiated by Yumita et al in 1989 (Yumita et al., 1989). Similar to photodynamic therapy (PDT), SDT uses low intensity ultrasound to stimulate sensitizers specifically accumulated in carcinoma cells to produce cytotoxic effects (Trendowski, 2014; Arakawa et al., 2002). Unlike the shallow penetration depth of visible light in PDT, ultrasound is clinically approved as a safe and valid imaging modality and can penetrate tens of centimeters deep into tissue layers and target at the site of malignancies, thereby overcomes the major penetration limitation of PDT (Wood and Sehgal, 2015; Wang et al., 2011).In addition, because the low toxicity of SDT, this treatment can be performed repeatedly without health concern, making it especially suitable for elderly and weak cancer patients who cannot undergo surgery or cannot tolerate radiotherapy or chemotherapy (Hu et al., 2015). Many experiments in vitro and in vivo had shown that SDT

Abbreviations: DVDMS, sinoporphyrin sodium; US, ultrasound; SDT, sonodynamic therapy; DVDMS-SDT, sinoporphyrin sodium-mediated sonodynamic therapy; PpIX, protoporphyrinIX; ROS, reactive oxygen species; NAC, N-acetylcysteine; DCFH-DA, 2′, 7′-dichlorofluorescin diacetate; CDK1, cyclindependent kinase 1; p21, cyclin-dependent kinase inhibitor 1A; BCL2, B-cell lymphoma 2; BAX, Bcl-2 Assaciated X protein; p53, tumor protein p53

* Corresponding authors at: Laboratory of Sono- and Photo-theranostic Technologies, Harbin Institute of Technology, Harbin, Heilongjiang, China.
E-mail addresses: huzheng@hit.edu.cn (Z. Hu), wcao@hit.edu.cn (W. Cao).

[1] These authors contribute equally to this work.

https://doi.org/10.1016/j.biocel.2019.01.009
Received 10 October 2018; Received in revised form 9 January 2019; Accepted 16 January 2019
Available online 17 January 2019
1357-2725/

could induce the apoptosis of tumor cells and reduce tumor growth rate (Osminkina et al., 2014; Li et al., 2018; Xie et al., 2018; Chen et al., 2017).

Recently, researchers have recognized that the sonosensitizer used is the key in the effectiveness of SDT. In practice, many photosensitizers used in photodynamic therapy were used in SDT, such as photofrin, haematoporphyrin, protoporphyrin, and hypocrellin, but their SDT effect is not ideal (Xu et al., 2013; Liu et al., 2007; Wang et al., 2012; Guo et al., 2013). Recently, a novel photosensitizer, sinoporphyrin sodium (DVDMS), a compound isolated from Photofrin II by Fang et al was developed (Fang and Yang (2012)). Compared with Photofrin II, the higher chemical purity, better water solubility, better targeting and shorter skin sensitivity period were achieved, indicating a good potential for clinical application of DVDMS in SDT (Liu et al., 2016).

Some previous studies showed that the DVDMS could be efficiently activated by ultrasound and inhibits tumor growth to a greater extent in several xenograft tumors (Hu et al., 2014; Wang et al., 2015a; Xiong et al., 2015), but the underlying mechanisms of DVDMS in SDT remains unclear. Moreover, DVDMS-mediated SDT (DVDMS-SDT) has not been investigated in HCC models up to date. Here, we focused our investigation on the anti-tumor effects of the sensitizer DVDMS combined with low intensity ultrasound to treat HCC both in vitro and in vivo.

2. Materials and methods

2.1. Sensitizers

DVDMS (molecular formula: C68H66N8O9Na4, Molecular weight: 1230.265, purity > 98%) and protoporphyrinIX (PpIX) were purchased from Qinglong Hi-tech Co, Ltd (Jiangxi, China). DVDMS was dissolved in double-distilled water to a stock concentration of 2 mg/ml and stored in the dark at −20 °C. The chemical structure of DVDMS is shown in Fig. 1.

2.2. Reagents and antibodies

3-(4,5-Dimethylthiazol-2-yl)-2,5-diphenyltertraz olium bromide tetrazolium (MTT), RNaseA, propidium iodide (PI), 2-(4-Amidinophenyl)-6-indolecarbamidine dihydrochloride (DAPI) and N-acetylcysteine (NAC) were obtained from Sigma (St Louis, MO, USA). 2′, 7′-dichlorofluorescin diacetate (DCFH-DA) was purchased from Molecular Probes Inc. (Eugene, OR, USA). Annexin V-FITC Apoptosis Kit was purchased from Biovision (Biovision, USA). Antibodies against BCL2, Bax, Cyclin B1, CDK1, CDK2, p21, p27, and β-actin were purchased from Santa Cruz Biotech (Santa Cruz, California, USA). Antibodies against p53 and Caspase-3 were obtained from Proteintech (Chicago, IL, USA). All other reagents were commercial products of analytical grade.

2.3. Cell culture

The human hepatocellular cell line Hep-G2 and human hepatocyte cell line HL-7702 (Chinese Academy of Sciences Institute of Cell Biology, Shanghai, China) were cultured in Dulbecco's modified Eagle's medium (DMEM; HyClone, Logan, UT, USA) supplemented with 10% fetal bovine serum (FBS; Thermo Fisher Scientific, Waltham, MA, USA) and penicillin–streptomycin–neomycin antibiotic mixture (1:100) (HyClone, Logan, UT, USA) in a 5% CO_2 humidified atmosphere at 37 °C.

2.4. Spectrophotometric and cellular uptake of DVDMS assay

The absorption spectra of DVDMS with a range of concentrations (10, and 20 μg/ml) in double-distilled water were recorded between 300 nm and 700 nm using a multi-volume spectrophotometer system (Epoch, BioTek, USA). In addition, the emission spectra of DVDMS were recorded at room temperature using a fluorescence microplate reader (Enspire, PE, USA). To investigate the cellular uptake of DVDMS, the differentiated Hep-G2 and HL-7702 cells were washed twice with phosphate buffered saline (PBS) and incubated with 10 μg/ml DVDMS in serum-free DMEM at 37 °C in the dark for 0–9 h. The cell medium was gently washed with PBS twice and observed using an Olympus IX-70 fluorescence microscope (Olympus, Tokyo, Japan). The fluorescence intensity of DVDMS was measured with a fluorescence spectrometer at 405 nm excitation and 624 nm emission wavelengths (USB2000; Ocean Optics Inc., Dunedin, FL, USA).

2.5. Ultrasonic system

The ultrasonic generator and power amplifier used in this study were designed and assembled by Harbin Institute of Technology (Harbin, China). *In vitro* (Fig. 2A), tumor cells were paved in a 3.5 cm diameter polystyrene cell culture dish and put inside a degassed water chamber above the 4.0 cm diameter ultrasonic transducer. Ultrasonic frequency of this apparatus was 0.84 MHz. The ultrasonic intensities of 0.25, 0.5, 0.75 W/cm^2 and duration of 120 s was used for treatments.

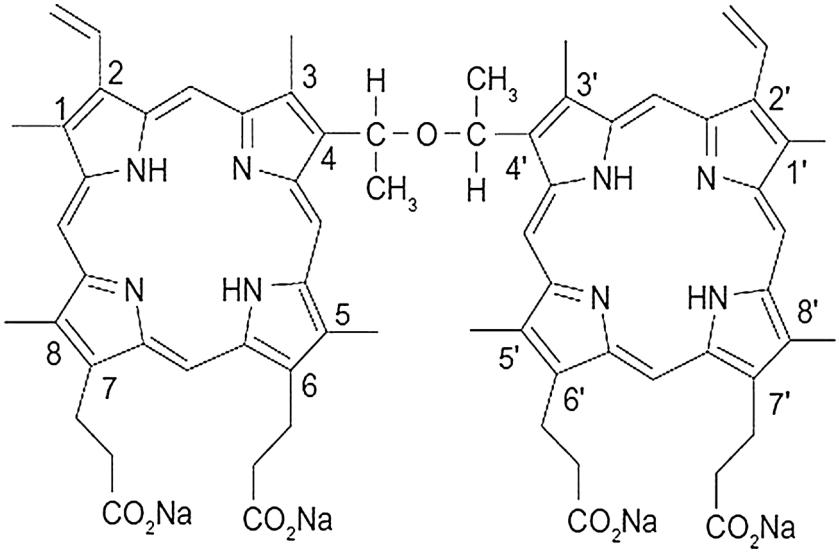

Fig. 1. The chemical structure of DVDMS.

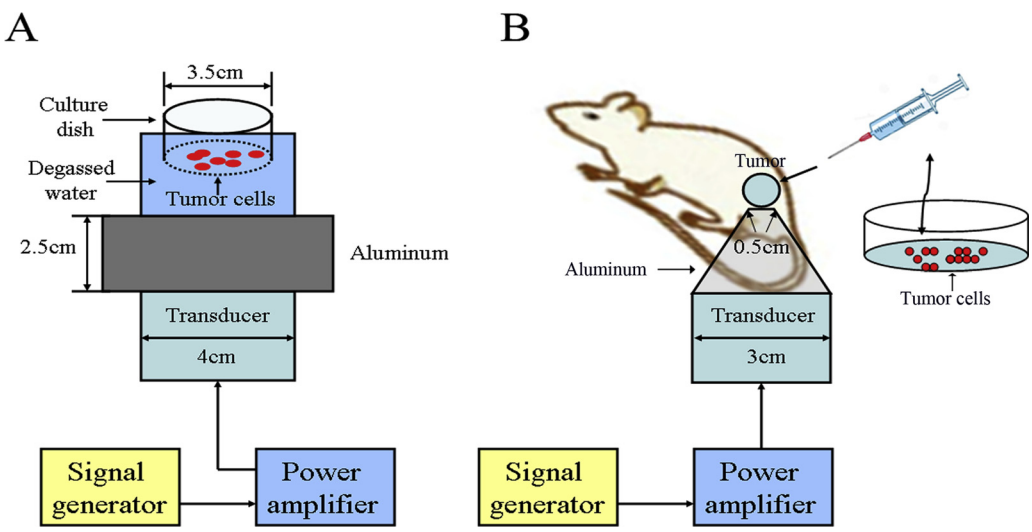

Fig. 2. Schematic diagram of low-intensity ultrasound device and the experimental setup. (A) The ultrasonic transducer was fixed by aluminum stents facing upward. The culture dish was placed above the center of the transducer for the in vitro experiments. (B) The ultrasound signal was applied through a tapered aluminum head with its front surface directly in contact with the mice skin above the tumor site through coupling grease for the in vivo experiments.

Cells were divided into 4 groups: control, sonosensitizer alone, ultrasound alone and SDT. For in vivo (Fig. 2B) experiments, a 3.0 cm diameter nonfocused ultrasonic transducer was attached to a tapered aluminum buffer head with a 0.5 cm diameter front surface, which was placed directly on the tumor of the mice with the ultrasonic coupling grease. The frequency of the ultrasound was 1.1 MHz, provided in tone-burst (TB) mode with a duty cycle of 10% and a repetition frequency of 100 Hz; ultrasonic intensity used was 1 W/cm^2. For the in vivo experiments, the temperature change was less than 2 °C in all experiments measured by a digital thermometer. Thus, any bio-effects observed in this study were considered to be non-thermal.

2.6. Cell viability assay

Cells were seeded at 1×10^4 cells/well in 96-well plates and incubated overnight. Cells were treated with sonosensitizer for 5 h and then exposed to ultrasound. After 24 h, MTT at 20 µl was added to each well and waited for another 4 h. The MTT mixture was removed and 150 µl DMSO was added to each well. The optical density (OD) was measured at 570 nm using a microplate reader (BioTek, Winooski, VT, USA). Cell proliferation was calculated using the following equation:

Cell proliferation (%) = OD treatment group/ OD control group $\times 100\%$

2.7. Apoptosis and cell cycle assay

Cells were harvested after different treatments and washed twice using cold PBS containing 0.5% BSA. For the apoptosis assay, cells were re-suspended in 1 × Binding Buffer and stained with 5 µL of annexin V-FITC and 5 µL of PI for 10 min in the dark. For the cell cycle assay, cell suspension was fixed in 1 ml 70% ethanol overnight, washed in PBS, and incubated at 37 °C for 30 min in the presence of 100 µl RNaseA, then mixed with 400 µl PI for 30 min. After staining, the samples were analyzed by flow cytometry (BD Biosciences, San Jose, CA, USA).

2.8. Intracellular ROS measurement

To study the roles of reactive oxygen species (ROS), cells were pretreated with 5 mM NAC (ROS scavenger) for 1 h prior to the sonication. Intracellular ROS production was measured by using reactive oxygen species assay kit (Applygen, Beijing, China). Briefly, 10 µM DCFH-DA diluents with DMEM were added to the Hep-G2 cells for 10 min at 37 °C. At 20 min incubation after the sonication, cells were harvested, washed three times with PBS, then examined using an Olympus IX-70 fluorescence microscope. Fluorescence images were taken at the excitation/emission wavelengths of 405/624 nm.

2.9. Western blot assay

Approximately 1×10^7 cells from each experimental group and control group were harvested, and RIPA lysis buffer [50 mM Tris−HCl pH 7.4, 150 mM NaCl, 1% (v/v) NP-40, 0.25% (w/v) sodium deoxycholate, and 0.5% (w/v) SDS] was added then cooled for 30 min on ice. The lysate was transferred to 1.5 ml Eppendorf tubes, homogenized, and then centrifuged at 12,000 × g for 30 min at 4 °C. The supernatant was transferred to a fresh tube and the Protein concentrations were determined using the BCA protein assay reagent (Beyotime, Jiangsu, China). The supernatants were mixed with equal volume of 2 × sodium dodecyl sulfate sample buffer and heated to 100°C for 10 min. An equal volume of sample (containing 50 µg of protein) was fractionated by SDS-PAGE on a 10% acrylamide gel and transferred onto a nitrocellulose membrane for 2 h. After blocking non-specific binding sites with 5% skimmed milk in TBST (50 mM Tris, 0.15 M NaCl, 0.1% Tween 20, pH 7.6) for 1 h, membranes were probed with primary antibodies at 4°C overnight, followed by incubation with horseradish peroxidase-conjugated secondary antibodies. The membrane was visualized with the enzymatic chemiluminescence kit (Pierce, Rockford, IL, USA).

2.10. Immunofluorescence

Five hours after the treatment, cells were fixed with 4% paraformaldehyde for 10 min and permeabilized with 0.5% Triton X-100 for 15 min. After 30 min of blocking in 1% BSA (dissolved in PBS and 0.05% Tween-20) at room temperature, cells were incubated with primary antibodies (1:100) overnight at 4 °C. Cy3-conjugated secondary antibody (1: 500; Beyotime, Shanghai, China) was added for 1 h followed by the addition of DAPI for 15 min. Finally, cells were examined using an Olympus IX-70 fluorescence microscope.

2.11. Tumor treatment model

Female BALB/c athymic nude mice (18–20 g body weight, 6–8 weeks of age) were obtained from SLAC Laboratory Animal Company (Shanghai, China). They were housed in an air-conditioned room at 23 °C ± 2 °C with free access to food and water and were maintained on a 12 h light-dark cycle. For the experiments, 1×10^6 Hep-G2 cells in 100 µl serum-free culture medium were subcutaneously injected into the right-side flanks of the mice. When the tumor grew to a volume of 100 mm^3, approximately 5 days after the implantation, mice were

randomly divided into 8 groups with 6 mice per group for two different experiments: (1) Evaluation of the anti-tumor efficacy. The four groups were as follows: Control, no stimulus; DVDMS, mice received 2 mg/kg DVDMS by Caudal vein injection; US, ultrasound alone and SDT group. The mice were euthanized 11 days after the treatments; (2) Survival analysis. The four groups were divided in the same way as in (1). The mice in the US and SDT groups were sonicated by ultrasound for 10 min. All experiments were performed in the dark to avoid optical excitation of DVDMS. Body weight and tumor growth were measured every day. Tumor diameter was determined by measuring the longest and shortest diameter with a vernier caliper, and the tumor volume (V) was calculated by the formula $V = \pi/6 \times L \times S^2$, where L and S are the long and short diameters of the tumor, respectively. Subcutaneous tumors were excised and fixed in buffered formalin for immunohistochemical analysis. All experiments were performed according to the standards supported by the Experimental Animal Care and Use Committee of Harbin Institute of Technology.

2.12. Immunohistochemical staining

After dewaxed and rehydrated, tissue sections went through antigen retrieval by heating in 10 mM citrate buffer (pH 6.0) for 3 min. Sections were immersed in 3% hydrogen peroxide solution for 10 min to quench endogenous peroxidase activity at room temperature. Non-specific binding was prevented by incubation with 5% normal goat serum for 10 min. The sections were stained with mouse anti-P53 (1:100 dilution), anti-Bax (1:50 dilution), anti-Bcl-2 (1:50 dilution), and anti-Cleaved-caspase-3 antibody (1:100 dilution) and incubated overnight at 4 °C. The sections were then incubated with secondary antibodies for 30 min at 37 °C. Sections were visualized using diaminobenzidine (DAB) (Zhongshan Goldenbridge, Beijing, China) solution counterstained with hematoxylin, and observed using light microscopy. Immunopositive tumor cells were randomly selected from 10 fields (magnification × 200) and quantified with integrated optical density (IOD) values by using Image-Pro Plus 5.0 (IPP, Media Cybernetics, Bethesda, MD, USA).

2.13. Statistical analysis

SPSS 19.0 sofware (SPSS Inc., Chicago) was used for statistical analysis. Data were presented as the means ± SD (standard deviation) based on at least three independent experiments. Differences among the groups were evaluated using one-way ANOVA, with $p < 0.05$ considered statistically significant.

3. Results

3.1. Spectrophotometric analysis and intracellular accumulation of DVDMS

Five absorption peaks had been detected at 405 nm, 506 nm, 541 nm, 574 nm and 622 nm, respectively, and the maximum peak was at approximately 405 nm (Fig. 3A). The peak at 624 nm was the maximum emission peak of DVDMS (Fig. 3B). The optimum uptake of DVDMS in Hep-G2 (cancerous) cells and HL-7702 (normal) cells was analyzed using fluorescence microscope and fluorescence spectrometer. After the treatment with 10 μg/ml of DVDMS, the fluorescence intensity increased gradually and reached the plateau at 5 h in Hep-G2 cells. Interestingly, compared with Hep-G2 cells, the fluorescence intensity reached a maximum after approximately 3 h in HL-7702 cells, and then rapidly decreased over a period of 4–9 h (Fig. 3C and D). Therefore, in our experiments, 5 h were chosen as the incubation time of DVDMS with cells.

3.2. Cell viability assessment

Hep-G2 cells were treated with different concentrations of DVDMS and different intensities of ultrasound (US). After 24 h, the MTT was performed. It was found that only at the highest DVDMS concentration of 3 μg/ml could one observe some inhibitive effect on cell with the viability of 86.48 ± 4.77% ($P < 0.05$ vs. Control), whereas other lower concentrations had no obvious effects on cell viability. Without DVDMS, US inhibited cell proliferation in an intensity-dependent manner. When the US intensity was 0.25, 0.5 and 0.75 W/cm^2, the cell viability decreased to 94.49 ± 5.36%, 87.69 ± 2.96% and 81.05 ± 3.28% ($P < 0.05$ vs. Control), respectively. The cell survival rate was significantly decreased when the cells were treated with combined 2.5 μg/ml of DVDMS plus 0.5 W/cm^2 of US, resulted in a maximum inhibitory effect on tumor cell growth with 76.4 ± 5.92% ($P < 0.01$ vs. Control). Thus, in the following experiments, we chose 2.5 μg/ml of DVDMS plus 0.5 W/cm^2 of US (DVDMS-SDT) as the treatment strategy (Fig. 4A).

To investigate the efficacy of DVDMS-SDT compared to PpIX-SDT, we also examined the cytotoxicity of PpIX-SDT (2.5 μg/ml of PpIX plus 0.5 W/cm2 of US). As shown in Fig. 4B, both DVDMS-SDT and PpIX-SDT could significantly inhibit Hep-G2 cells proliferation. However, reduction in cell viability is much stronger in DVDMS-SDT than in PpIX-SDT (reduction of 62.93 ± 3.52% vs. 49.43 ± 2.68%). Further more; neither DVDMS nor PpIX alone caused any negative effect on normal cell viability in HL-7702 cells, while PpIX-SDT group exhibited higher level of inhibition than that of the DVDMS-SDT group.

3.3. Apoptosis detection

Apoptotic rates were measured by Annexin V-FITC/PI staining after various treatments. As shown in Fig. 5A, there were 4.4 ± 1.2% and 7.9 ± 1.7% ($P < 0.05$ vs. Control) apoptosis cells in DVDMS and PpIX groups, respectively and 5.5 ± 1.3% apoptosis cells were found in the US alone group. In the DVDMS-SDT and PpIX-SDT groups, the proportion of apoptosis cells increased to 32.4 ± 3.7% ($P < 0.01$ vs. PpIX-SDT) and 15.3 ± 2.6% ($P < 0.01$ vs. Control), respectively. These results indicated that DVDMS is a more potent sonosensitiser than PpIX. In addition, we also investigated the apoptosis of HL-7702 cells after the DVDMS-SDT treatment. As shown in Fig. 5B, we found that, in contrast with Hep-G2 cells, no significant apoptosis was observed in HL-7702 cells. Hence, the procedure is safe for normal cells, implying no side effects during cancer treatment using DVDMS-SDT.

3.4. DVDMS-SDT induced G2/M phase arrest

The effect of DVDMS-SDT on cell cycle distribution was evaluated by flow cytometry in Hep-G2 cells. As shown in Fig. 6A and B, DVDMS or US alone had no obvious cell cycle changes compared to that of the Control group. However, the DVDMS-SDT group revealed an increasing tendency in the percentage of cells in the G2/M phase (18.23 ± 3.74%, $P < 0.01$ vs. Control), while a reduction in the percentage of cells in the G0/G1 phase (44.39 ± 4.12%, $P < 0.05$ vs. Control). CDKs and Cyclins, as cell cycle regulators, play an important role in cell cycle progression. Cell-cycle progression is accelerated by cyclins and CDKs, and decelerated by CDK inhibitors (such as p21 and p27). To investigate the mechanisms by which DVDMS-SDT induced G2/M phase arrest, we performed western blot analysis to evaluate Cyclin B1, CDK1, CDK 2 and CDK inhibitor protein p21 and p27. As shown in Fig. 6C, the p21 and p27 levels increased after DVDMS-SDT treatment. In contrast, the levels of Cyclin B1 and CDK1 decreased, whereas the DVDMS-SDT treatment did not affect CDK2 expression. Meanwhile, we found that DVDMS-SDT had no effect on the cell cycle in HL-7702 cells (Supplementary Fig. 1A and B).

3.5. The cytotoxicity of DVDMS-SDT are mediated by ROS production

Previous studies had verified that SDT-induced cell death is closely related to the generation of intracellular ROS (Su et al., 2015; You et al.,

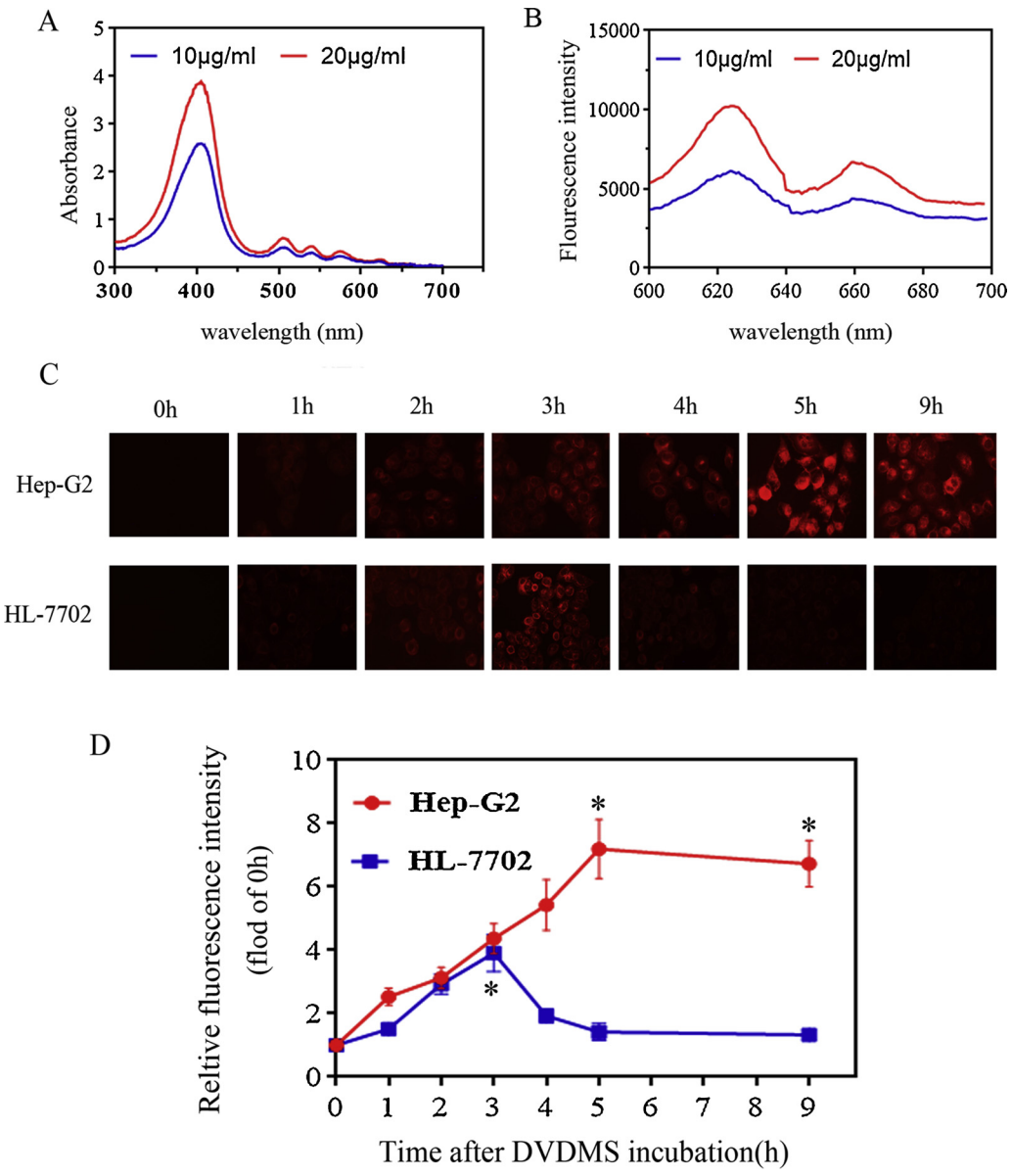

Fig. 3. Spectrophotometric analysis and Cellular uptake of DVDMS. (A) The absorption spectra of DVDMS were detected by multi-volume spectrophotometer system in double-distilled water. (B) The emission spectra of DVDMS were detected by fluorescence microplate reader in double-distilled water. (C) The accumulation of DVDMS in Hep-G2 cells and HL-7702 cells were detected by fluorescent microscope (magnification × 400) at different time-point after incubation with 10 μg/ml DVDMS. (D) The fluorescence intensity of DVDMS in Hep-G2 cells and HL-7702 cells were detected by fluorescence spectrometer. *P < 0.05 vs. Control. Data are means ± SD of three independent experiments.

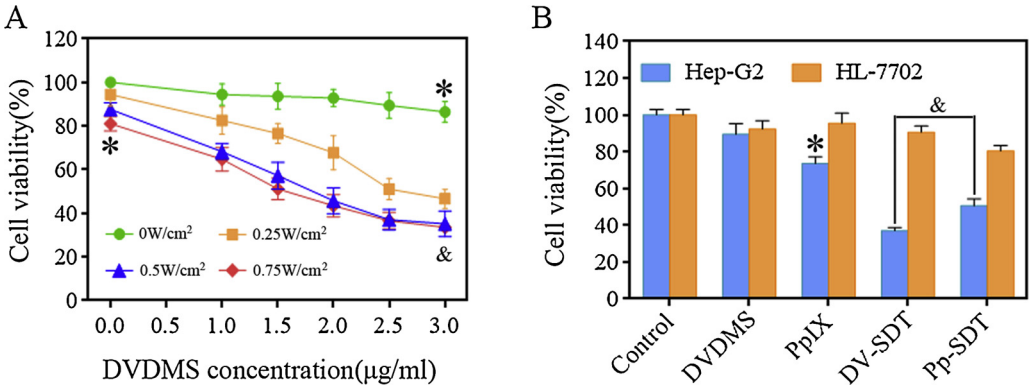

Fig. 4. Cell viability assessment. (A) Hep-G2 cells were treated with different concentrations of DVDMS at 0–3 μg/ml, different intensities of US at 0-0.75 W/cm^2 and DVDMS plus US. Cell viability was determined by MTT assay. *P < 0.05 vs. control, and & P < 0.01 vs. control. (B) Cell viability for Hep-G2 cells and HL-7702 cells treated with 2.5 μg/ml of DVDMS or PpIX plus US. *P < 0.05 vs. Control, and P < 0.05 between groups. Data are means ± SD of three independent experiments.

2016). Therefore, we monitored intracellular ROS levels using DCFH-DA staining after different treatments. As shown in Fig. 7A, the green fluorescence intensities increased following DVDMS-SDT compared with the Control, DVDMS or US alone groups, indicating significant increase of the intracellular ROS level in Hep-G2 cells. Conversely, the production of ROS was effectively blocked by the ROS scavenger, NAC.

To further investigate the role of ROS in SDT-induced cell apoptosis in Hep-G2 cells, cells were pretreated with NAC. As shown in Fig. 7B, the apoptosis rate of Hep-G2 cells in the SDT group increased to 32.4 ± 3.7% (P < 0.01 vs. Control), which was significantly higher compared to that of other groups, while the NAC showed the potential to significantly reduce the apoptosis induced by the SDT treatment

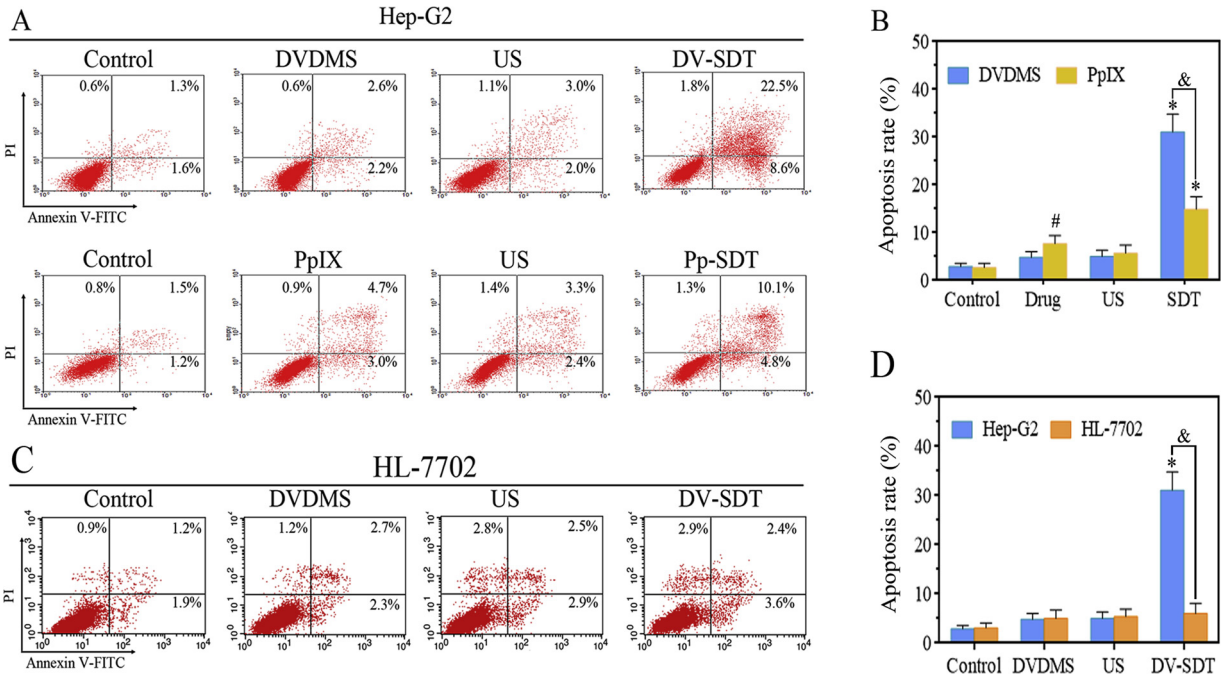

Fig. 5. Apoptosis detection. (A) Induction of apoptosis after different treatments in Hep-G2 cells. Cells in the lower-left quadrant represented viable cells, both the lower-right and upper-right quadrant showed the apoptotic cells, and the necrotic cells appeared in the upper-left quadrant. (B) The rate of apoptosis of Hep-G2 cells determined by FCM assay. Drug represents DVMDS alone or PPIX alone. $^{\#}P < 0.05$ vs. Control, $^{*}P < 0.01$ vs. Control and $^{\&}P < 0.01$ between groups. (C) Induction of apoptosis after different treatments in HL-7702 cells. (D) The rate of apoptosis of Hep-G2 cells and HL-7702 cells determined by FCM assay. $^{*}P < 0.01$ vs. Control and $^{\&}P < 0.01$ between groups. Data are means ± SD of three independent experiments.

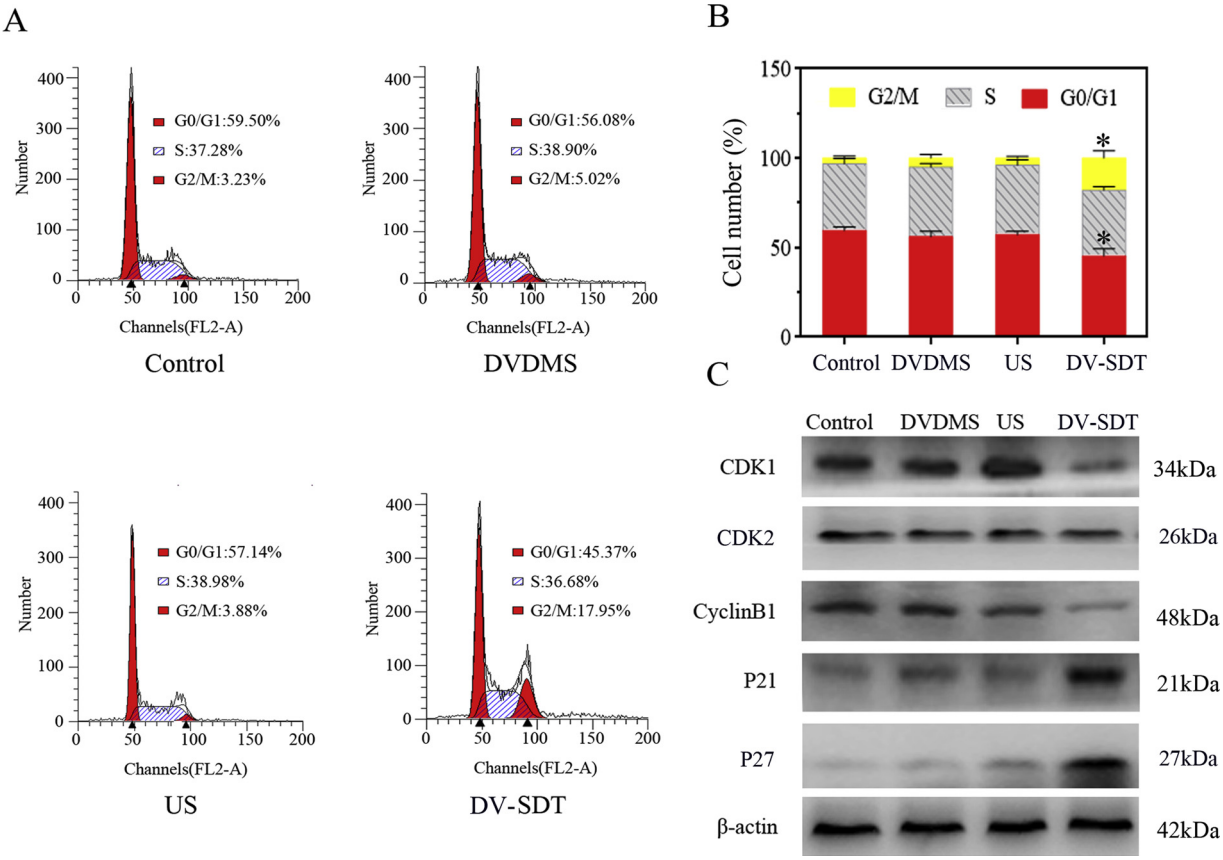

Fig. 6. Cell cycle analysis of Hep-G2 cells after different treatments. (A) The percentages of cell cycle distribution of different groups were analyzed using flow cytometry. (B) Histogram represents the percentage of cells arrested in different phases of cell cycle. $^{*}P < 0.01$ vs. Control. (C) The expression level of Cyclin B1, CDK1, CDK2, P21 and P27 was determined by Western blot. β-actin served as loading control. Data are means ± SD of three independent experiments.

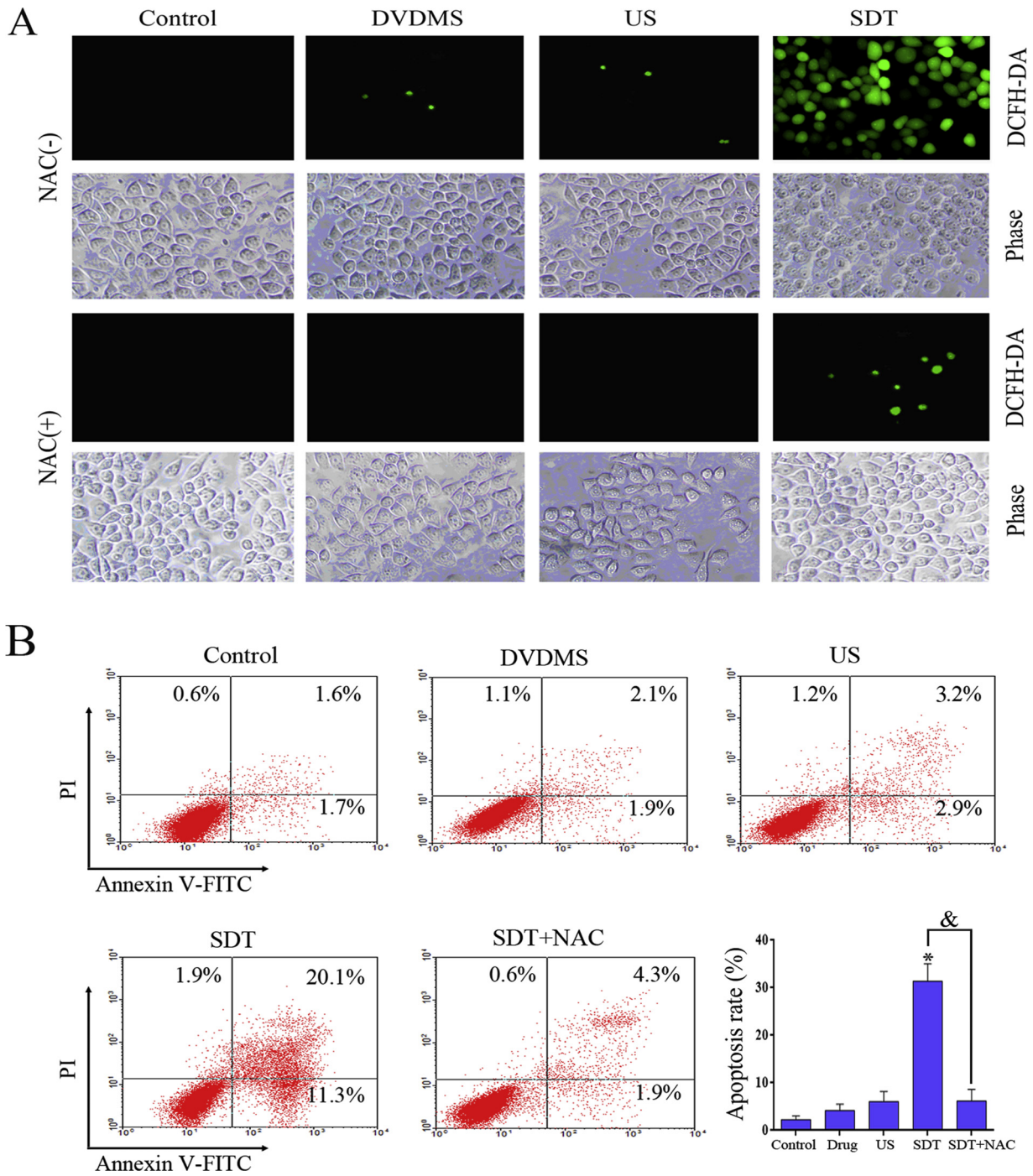

Fig. 7. The cytotoxicity of DVDMS-SDT is mediated by ROS production. (A) The levels of intracellular ROS induced by ALA-SDT in vitro. The cells were labeled with DCFH-DA and observed by fluorescence microscopy (magnification × 400). Green fluorescence indicates the level of intracellular ROS. (B) Induction of apoptosis after different treatments in Hep-G2 cells. The apoptosis rate of Hep-G2 cells determined by FCM assay. *P < 0.01vs. Control and $^{\&}$P < 0.01 between groups. Data are means ± SD of three independent experiments (For interpretation of the references to colour in this figure legend, the reader is referred to the web version of this article).

down to 5.9 ± 2.4% (P < 0.01 vs. DVDMS-SDT).

3.6. DVDMS-SDT regulated the expression of apoptosis related proteins via ROS

In order to explore the signaling pathway(s) mediating the inhibitory effect of DVDMS-SDT on Hep-G2 cells growth, we measured the changes in the protein expression of p53, Caspase-3, Bax and Bcl-2 after different treatment by western blot analysis. As shown in Fig. 8A, the Control, DVDMS and US group have no significant difference, but in the DVDMS-SDT group, p53, cleaved caspase-3 and Bax expressions were increased to 572.3 ± 33.3, 648.3 ± 28.2%, and 604.6 ± 25.7%, respectively (p < 0.01 vs. other three groups), whereas Bcl-2 expression was decreased to 30.2 ± 7.2% (p < 0.01 vs. the other three groups). When treated with NAC, the expression of these proteins was almost recovered (Fig. 8B). We also investigated the distribution of apoptosis-related proteins by Immunofluorescence staining. As shown in Fig. 8C, in the control group, p53 mainly distributed in the

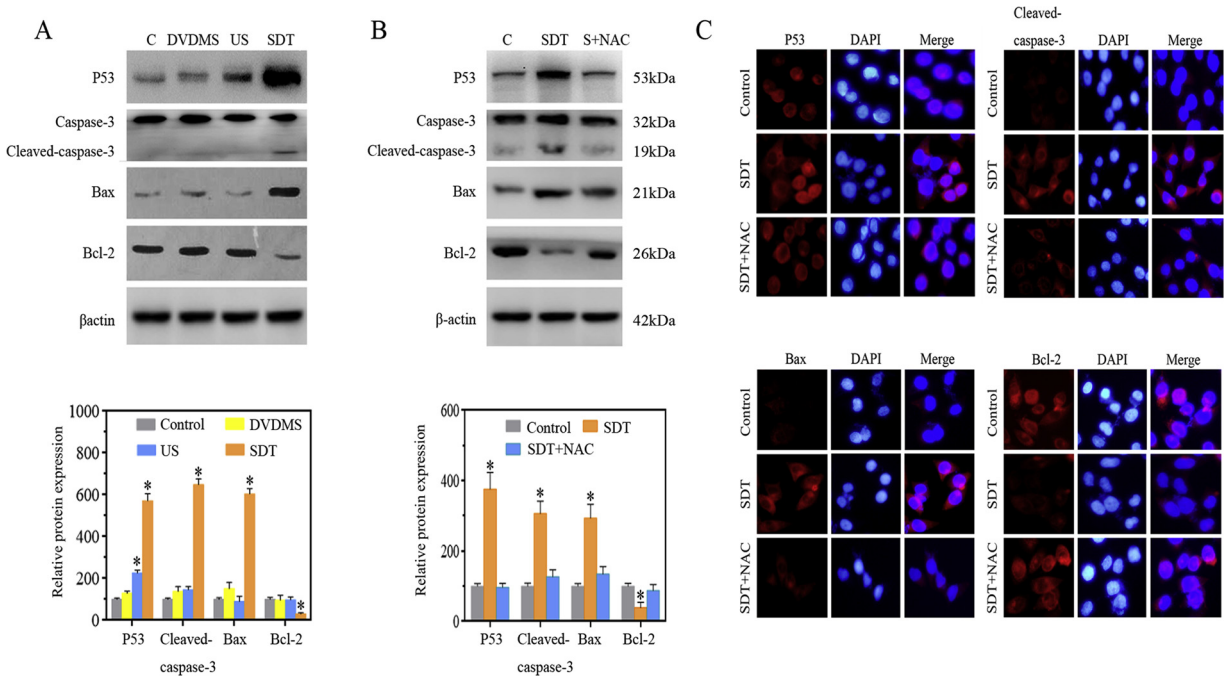

Fig. 8. DVDMS-SDT regulated the expression of apoptosis related proteins via ROS. (A) The expression levels of p53, Caspase-3, Bax, and Bcl-2 were determined by Western blot in Hep-G2 cells. β-actin served as the loading control. (B) Representative expression of apoptosis-related proteins with and without NAC in Hep-G2 cells. Histogram represents the percentages of relative protein expression in different treatment groups. *P < 0.01 vs. Control. (C) The cells were stained with antibodies of apoptosis-related proteins (red), and nuclei were stained with DAPI. Images were captured by fluorescence microscopy (magnification × 400). Data are means ± SD of three independent experiments (For interpretation of the references to colour in this figure legend, the reader is referred to the web version of this article).

nuclei and cleaved caspase-3, while Bax and Bcl-2 primarily distributed in the cytoplasm. Following the treatment with DVDMS-SDT, cleaved caspase-3, Bax and Bcl-2 remained in the cytoplasm, while p53 distributed in the nuclei and cytoplasm. The fluorescence intensities of p53, cleaved caspase-3 and Bax were increased compared to that of the control group and the Bcl-2 fluorescence was decreased. Furthermore, these fluorescence changes were partially recovered by NAC. Meanwhile, we found that DVDMS-SDT had no effect on the apoptosis-related protein levels in HL-7702 cells (Supplementary Fig. 1C).

Taken together, these results indicated that the DVDMS-SDT indeed induced caspase-dependent apoptosis via ROS.

3.7. DVDMS-SDT suppressed tumor growth and prolonged the survival time of BALB/c athymic nude mice

Having determined the effect of DVDMS-SDT on Hep-G2 cells in vitro, the next step is to evaluate the effect of this treatment in vivo. Hep-G2 cells were injected subcutaneously into the right flanks of BALB/c mice. The effect of different treatment strategies was quantified by measuring the tumor size. The tumor volumes in all groups were about the same before the treatment. As shown in Fig. 9A and Supplementary Fig. 2, a significant tumor growth inhibition for animals treated using DVDMS-SDT was observed (P < 0.01 vs. Control), with the mean tumor size of 294.4 ± 31.4 mm^3 at day 11. By contrast, there was no significant inhibition effect on tumor growth for the DVDMS group and a little anti-tumor effect for the US group, with the mean tumor size of 959.2 ± 82.1 mm^3 and 765.7 ± 72.6 mm^3, respectively, over the same time period. Moreover, the weight curve of mice in Fig. 9B testified that the mice weight had no noticeable change over the course of the experiment. Fig. 9C and D showed the results of the Kaplan–Meier survival for all groups. US alone group slightly prolonged the survival of the Hep-G2 hepatic cancer-bearing mice (25 ± 0.6 days, P < 0.05 vs. Control), whereas the survival period in the DVDMS-SDT group (35.3 ± 1.1 days) was significantly longer than all other groups (p < 0.01).

3.8. Immunohistochemical observation

Western blot analysis in vitro of apoptosis related proteins expression is shown in Fig. 8A. Similar results were achieved by immunohistochemical staining in vivo as shown in Fig. 10A and B, which also revealed that the DVDMS-SDT group exhibited increased P53, Cleaved-caspase-3, and Bax expression levels and decreased Bcl-2 expression compared to the other three groups (P < 0.01).

4. Discussion

High selectivity and noninvasive target cancer treatments are urgently needed for hepatocellular carcinoma due to the disadvantages of conventional therapies, such as low selectivity and long-term side effects (Dy and Adjei (2013)). Sonodynamic therapy, a noninvasive therapeutic strategy, represents a promising approach in cancer treatments. In recent years, SDT has been widely investigated in the field of cancer treatment (Trendowski (2014)). But there are no literature reports about the DVDMS as a sonosentizer to mediate the SDT in treating HCC. In the present study, we have investigated the efficacy and mechanisms of DVDMS mediated SDT as a treatment strategy for HCC.

Treating cancers using SDT is based on preferential uptake and/or retention of sonosensitizer in tumor tissues and subsequent activation of the drug by low intensity ultrasound, specifically causing tumor apoptosis (Wang et al., 2014). Previous studies indicated that DVDMS in S180 sarcoma cells reached a peak at 2 h, and the DVDMS concentrations at 6 h and 24 h of DVDMS were about 98.77% and 70.37% of the peak, respectively (Li et al., 2014). In this study, we confirmed that the cellular uptake of DVDMS reached the maximum when the DVDMS incubated with Hep-G2 cells for 5 h, and with HL-7702 cells for 3 h, then rapidly decreased over a period of 4–9 h (Fig. 3C and D). These results suggested that normal cells metabolized sonosensitizer faster

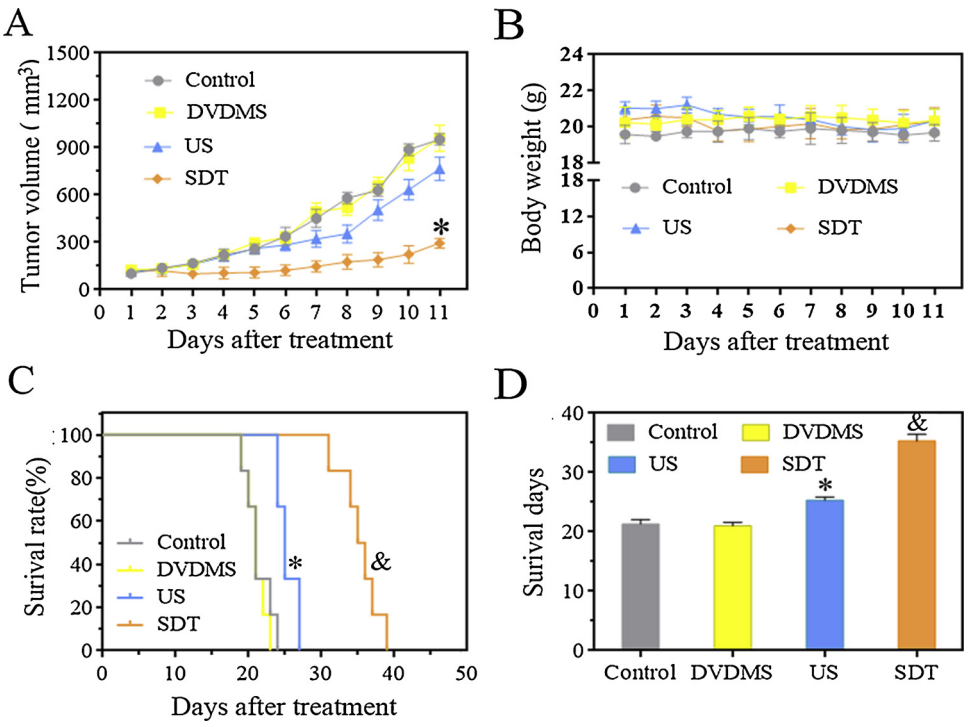

Fig. 9. DVDMS-SDT suppressed tumor growth and prolonged the survival time of BALB/c athymic nude mice. (A) Tumor-bearing nude mice in the Control, DVDMS, US and DVDMS-SDT groups. *P < 0.01 vs. Control. (B) A plot of body weight versus the number of days post different treatments. (C and D) Overall survival analysis results by the Kaplan-Meier survival curves (log-rank test). *p < 0.05 vs. Control and &p < 0.01 vs. other three groups. Data was presented as the mean ± SD (n = 6).

than HCC cells, so that the optimal treatment time of DVDMS with cells was chosen to be 5 h.

A sonosensitizer with high ultrasound sensitivity is essential for efficient SDT. Our viability assessment results showed that DVDMS-SDT could significantly inhibit Hep-G2 cell proliferation in a drug dose and ultrasound intensity dependent manner (Fig. 4A). Under the same treatment conditions, DVDMS-SDT exhibited a higher efficacy than PpIX-SDT in inhibiting the growth of Hep-G2 cells, but the opposite occurred with HL-7702 cells (Fig. 4B). The results were further supported by apoptosis assay. The apoptosis rate of Hep-G2 cells was 31.1 ± 3.7% in DVDMS-SDT group, but was only 14.9 ± 2.6% in PpIX-SDT group. In addition, no obvious apoptosis were observed in HL-7702 cells after the DVDMS-SDT treatment (Fig. 5). These findings indicated that DVDMS is a more potent sonosensitiser than PpIX.

There were limited studies in the literature on SDT inducing cell cycle changes. Li et al. (2008) found that 0.5 W/cm^2 ultrasound plus HMME increased the percentage of C6 cells in the S phase. High energy shock waves combined with ALA were able to induce HT-29 cells arrest in the G0/G1 phase (Canaparo et al., 2006). We found that DVDMS-SDT resulted in the G2/M phase arrest (Fig. 6A), decreased CDK1 and Cyclin B1, and increased CDK inhibitor p21 protein expressions (Fig. 6C). Our results demonstrated that the DVDMS-SDT inhibits the proliferation of Hep-G2 cells might be associated with the G2/M cell cycle arrest.

It is well known that the production of ROS is one of the vital mechanisms of PDT and might be also involved in SDT (Wang et al., 2015b). Here, we detected that the ROS level was significant increased and the cell apoptosis could be reversed in the presence of NAC after the DVDMS-SDT treatment (Fig. 7). These results suggested that the production of ROS was indeed involved in the anti-cancer effect of DVDMS-SDT because ROS, as an effective oxidant, directly regulate the function

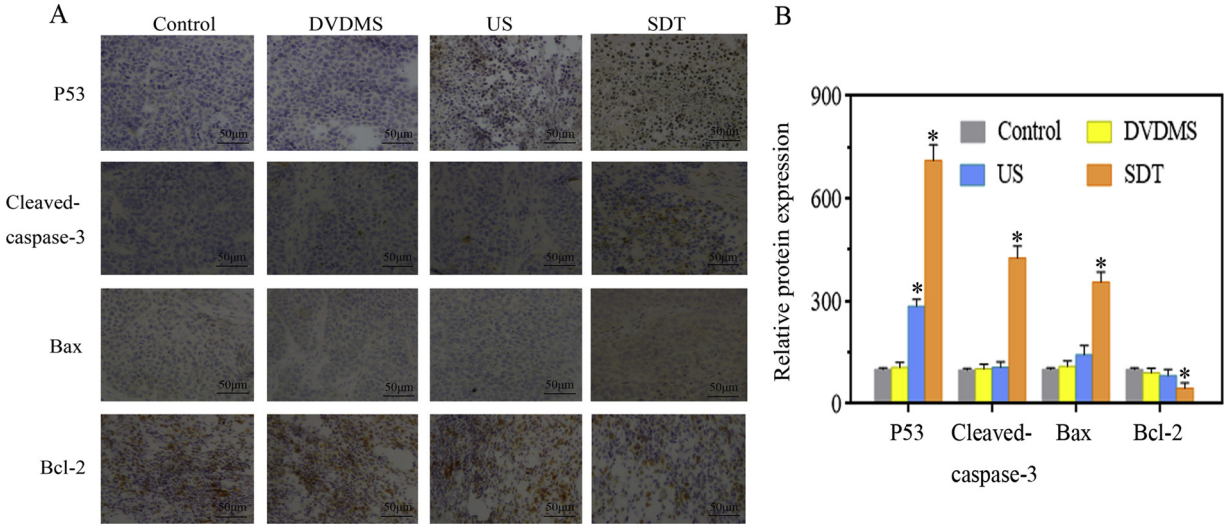

Fig. 10. Immunohistochemistry detection for apoptosis related proteins after different treatments. (A) Immunohistochemistry was used to detect the expression levels of p53, Bcl-2, Bax, and Cleaved-caspase-3. (B) Relative protein expression was calculated by Image Pro Plus 6.0 (Media Cybernetics, Inc., Bethesda, MD, USA) with integrated optical density (IOD) values. *P < 0.01 vs. other three groups. Data was presented as the mean ± SD (n = 6).

of proteins, transcription factors and genes (Trachootham et al. (2009)). Multiple reports have indicated that excessive levels of ROS stress gave rise to the apoptosis of SDT-treated cells (Yumita et al. (2012); Yumita et al., 2010). It was reported that ROS could upregulate p53 through the induction of apoptosis and subsequent trigger the pro-apoptotic factor-Bax and the antiapoptotic factor-Bcl-2 (Hwang et al., 2001; Chumakova et al., 2006). Chumakova Bax associated with caspase-3 to activate the mitochondria-caspase pathway lead to cellular apoptosis (Adachi et al., 1999). In this study, our results indicated that the DVDMS-SDT in vitro increased the expressions of p53, cleaved caspase-3 and Bax, while decreased the expressions of Bcl-2 (Fig. 8A). Supporting results were achieved by immunohistochemical staining in vivo (Fig. 10). These changes could be partially rescued by the ROS scavenger NAC in vitro (Fig. 8B). Thus, we believe that the increased ROS production caused by DVDMS-SDT regulated the expression of apoptosis related proteins, resulted in tumor cell apoptosis.

Because the low intensity ultrasound can penetrate deep into the tissue regardless of the tumor location, we were also performed experiments in vivo. Animal studies confirmed that the tumor volume in SDT group was significantly inhibited in comparison with the Control, DVDMS and Ultrasound alone groups (Fig. 9A). There was no obvious body weight reduction during the whole treatment period (Fig. 9B). The DVDMS-SDT also markedly prolonged the survival of the Hep-G2 hepatic cancer-bearing mice (Fig. 9C and D).

In Conclusion, Our results in this work suggested that the DVDMS-SDT could significantly inhibit Hep-G2 cells proliferation and induce cell apoptosis in vitro, and inhibit tumor growth in vivo. The primary mechanism was via the increased ROS level activated the p53-caspase-3 pathway of apoptosis. In addition, the procedure is safe to normal cells. All of these results show that the DVDMS-SDT is an effective therapeutic strategy for treating HCC.

Conflict of interest

The authors declare that they have no conflict of interest.

Acknowledgements

This work was supported by grants from the National Natural Science Foundation of China (Grant No. 81571720 and 81702925), the Natural Science Foundation of Heilongjiang Province (Grant No. H201403 and H2018002), the Science and Technology Research Project of Education Department of Heilongjiang Province (Grant No. 12541447), and the China Postdoctoral Science Foundation (Grant No. 2016M591551).

Appendix A. Supplementary data

Supplementary material related to this article can be found, in the online version, at doi:https://doi.org/10.1016/j.biocel.2019.01.009.

References

Adachi, Y., Taketani, S., Oyaizu, H., Ikebukuro, K., Tokunaga, R., Ikehara, S., 1999. Apoptosis of colorectal adenocarcinoma induced by 5-FU and/or IFN-gamma through caspase 3 and caspase 8. Int. J. Oncol. 15, 1191–1196.

Arakawa, K., Hagisawa, K., Kusano, H., Yoneyama, S., Kurita, A., Arai, T., Kikuchi, M., Sakata, I., Umenura, S., Ohsuzu, F., 2002. Sonodynamic therapy decreased neointimal hyperplasia after stenting in the rabbit iliac artery. Circulation 105, 149–151.

Bruix, J., Takayama, T., Mazzaferro, V., Chau, G.Y., Yang, J.M., Kudo, M., Cai, J.Q., Poon, R.T., Han, K.H., Tak, W.Y., Lee, H.C., Song, T.Q., Roayaie, S., Bolondi, L., Lee, K.S., Makuuchi, M., Souza, F., Le Berre, M.A., Meinhardt, G., Llovet, J.M., Investigators, S., 2015. Adjuvant sorafenib for hepatocellular carcinoma after resection or ablation (STORM): a phase 3, randomised, double-blind, placebo-controlled trial. Lancet Oncol. 16, 1344–1354.

Canaparo, R., Serpe, L., Catalano, M.G., Bosco, O., Zara, G.P., Berta, L., Frairia, R., 2006. High energy shock waves (HESW) for sonodynamic therapy: effects on HT-29 human colon cancer cells. Anticancer Res. 26, 3337–3342.

Chen, L., Cong, D.M., Li, Y.Z., Wang, D., Li, Q.S., Hu, S.S., 2017. Combination of sonodynamic with temozolomide inhibits C6 glioma migration and promotes mitochondrial pathway apoptosis via suppressing NHE-1 expression. Ultrason. Sonochem. 39, 654–661.

Chumakova, O.V., Liopo, A.V., Evers, B.M., Esenaliev, R.O., 2006. Effect of 5-fluorouracil, optison and ultrasound on MCF-7 cell viability. Ultrasound Med. Biol. 32, 751–758.

Dy, G.K., Adjei, A.A., 2013. Understanding, recognizing, and managing toxicities of targeted anticancer therapies. CA Cancer J Clin 63, 249–279.

Fang Q., Yang D., A porphyrin dimer combined with an ether bond and its manufacturing method. People's Republic of China y. 2012; Patent ZL 200910179116.5.

Guo, S.Y., Sun, X., Cheng, J.L., Xu, H.B., Dan, J.H., Shen, J., Zhou, Q., Zhang, Y., Meng, L.L., Cao, W.W., Tian, Y., 2013. Apoptosis of THP-1 macrophages induced by protoporphyrin IX-mediated sonodynamic therapy. Int. J. Nanomed. Nanosurg. 8, 2239–2246.

Hu, J.M., Wang, X.B., Zhang, K., Wang, P., Su, X.M., Li, Y.X., Huang, Z.X., Liu, Q.H., 2014. Sinoporphyrin sodium: a novel sensitizer in sonodynamic therapy. Anti-Cancer Drug 25, 174–182.

Hu, Z., Fan, H.X., Lv, G.X., Zhou, Q., Yang, B., Zheng, J.H., Cao, W.W., 2015. 5-Aminolevulinic acid-mediated sonodynamic therapy induces anti-tumor effects in malignant melanoma via p53-miR-34a-Sirt1 axis. J. Dermatol. Sci. 79, 155–162.

Hwang, P.M., Bunz, F., Yu, J., Rago, C., Chan, T.A., Murphy, M.P., Kelso, G.F., Smith, R.A.J., Kinzler, K.W., Vogelstein, B., 2001. Ferredoxin reductase affects p53-dependent, 5-fluorouracil-induced apoptosis in colorectal cancer cells. Nat. Med. 7, 1111–1117.

Li, J.H., Song, D.Y., Xu, Y.G., Huang, Z., Yue, W., 2008. In vitro study of haematoporphyrin monomethyl ether-mediated sonodynamic effects on C6 glioma cells. Neurol. Sci. 29, 229–235.

Li, C.F., Zhang, K., Wang, P., Hu, J.M., Liu, Q.J., Wang, X.B., 2014. Sonodynamic antitumor effect of a novel sonosensitizer on S180 solid tumor. Biopharm. Drug Dispos. 35, 50–59.

Li, M.F., Guan, H., Zhang, D.D., 2016. Effect of overexpression of PTEN on apoptosis of liver cancer cells. Genet. Mol. Res. 15.

Li, Z.L., Han, J., Yu, L.D., Qian, X.Q., Xing, H., Lin, H., Wu, M.C., Yang, T., Chen, Y., 2018. Synergistic sonodynamic/chemotherapeutic suppression of hepatocellular carcinoma by targeted biodegradable mesoporous nanosonosensitizers. Adv. Funct. Mater. 28.

Liu, Q.H., Wang, X.B., Wang, P., Xiao, L.N., Hao, Q., 2007. Comparison between sonodynamic effect with protoporphyrin IX and hematoporphyrin on sarcoma 180. Cancer Chemother. Pharm. 60, 671–680.

Liu, Y.C., Wang, P., Liu, Q.H., Wang, X.B., 2016. Sinoporphyrin sodium triggered sonophotodynamic effects on breast cancer both in vitro and in vivo. Ultrason. Sonochem. 31, 437–448.

Ma, S.S., Sun, J.Z., Guo, Y.B., Zhang, P., Liu, Y.X., Zheng, D.X., Shi, J., 2017. Combination of AAV-TRAIL with miR-221-Zip therapeutic strategy overcomes the resistance to TRAIL induced apoptosis in liver Cancer. Theranostics 7, 3228–3242.

Osminkina, L.A., Sivakov, V.A., Mysov, G.A., Georgobiani, V.A., Natashina, U.A., Talkenberg, F., Solovyev, V.V., Kudryavtsev, A.A., Timoshenko, V.Y., 2014. Nanoparticles prepared from porous silicon nanowires for bio-imaging and sonodynamic therapy. Nanoscale Res. Lett. 9.

Roayaie, S., Jibara, G., Tabrizian, P., Park, J.W., Yang, J.J., Yan, L.N., Schwartz, M., Han, G.H., Izzo, F., Chen, M., Blanc, J.F., Johnson, P., Kudo, M., Roberts, L.R., Sherman, M., 2015. The role of hepatic resection in the treatment of hepatocellular cancer. Hepatology 62, 440–451.

Su, X.M., Wang, P., Yang, S., Zhang, K., Liu, Q.H., Wang, X.B., 2015. Sonodynamic therapy induces the interplay between apoptosis and autophagy in 1062 cells through ROS. Int. J. Biochem. Cell B (60), 82–92.

Torre, L.A., Bray, F., Siegel, R.L., Ferlay, J., Lortet-Tieulent, J., Jemal, A., 2012. Global Cancer statistics. CA-Cancer J. Clin. 2015 (65), 87–108.

Trachootham, D., Alexandre, J., Huang, P., 2009. Targeting cancer cells by ROS-mediated mechanisms: a radical therapeutic approach? Nat. Rev. Drug Discov. 8, 579–591.

Trendowski, M., 2014. The promise of sonodynamic therapy. Cancer Metast Rev. 33, 143–160.

Wang, J., Guo, Y.W., Gao, J.Q., Jin, X.D., Wang, Z.Q., Wang, B.X., Li, K., Li, Y., 2011. Detection and comparison of reactive oxygen species (ROS) generated by chlorophyllin metal (Fe, Mg and Cu) complexes under ultrasonic and visible-light irradiation. Ultrason. Sonochem. 18, 1028–1034.

Wang, X.N., Leung, A.W., Jiang, Y., Yu HP, Li X.H., Xu, C.S., 2012. Hypocrellin B-mediated sonodynamic action induces apoptosis of hepatocellular carcinoma cells. Ultrasonics 52, 543–546.

Wang, H.P., Wang, X.B., Zhang, S.L., Wang, P., Zhang, K., Liu, Q.H., 2014. Sinoporphyrin sodium, a novel sensitizer, triggers mitochondrial-dependent apoptosis in ECAECA-109 cells via production of reactive oxygen species. Int. J. Nanomed. Nanosurg. 9, 3077–3090.

Wang, H.P., Wang, P., Li, L., Zhang, K., Wang, X.B., Liu, Q.H., 2015a. Microbubbles enhance the antitumor effects of sinoporphyrin sodium mediated sonodynamic therapy both in vitro and in vivo. Int. J. Biol. Sci. 11, 1401–1409.

Wang, P., Li, C.F., Wang, X.B., Xiong, W.L., Feng, X.L., Liu, Q.H., Leung, A.W., Xu, C.S., 2015b. Anti-metastatic and pro-apoptotic effects elicited by combination photodynamic therapy with sonodynamic therapy on breast cancer both in vitro and in vivo. Ultrason. Sonochem. 23, 116–127.

Wood, A.K.W., Sehgal, C.M., 2015. A review of low-intensity ultrasound for Cancer therapy. Ultrasound Med. Biol. 41, 905–928.

Xie, L.F., Feng, X.L., Shi, Y., He, M., Wang, P., Wang, X.B., Mi, Z.Y., Liu, Q.H., Zhang, K., 2018. Blocking the glycolytic pathway sensitizes breast Cancer to sonodynamic therapy. Ultrasound Med. Biol. 44, 1233–1243.

Xiong, W.L., Wang, P., Hu, J.M., Jia, Y.L., Wu, L.J., Chen, X.Y., Liu, Q.H., Wang, X.B., 2015. A new sensitizer DVDMS combined with multiple focused ultrasound treatments: an effective antitumor strategy. Sci. Rep. 5.

Xu, Z.Y., Wang, K., Li, X.Q., Chen, S., Deng, J.M., Cheng, Y., Wang, Z.G., 2013. The ABCG2 transporter is a key molecular determinant of the efficacy of sonodynamic therapy with Photofrin in glioma stem-like cells. Ultrasonics 53, 232–238.
You, D.G., Deepagan, V.G., Um, W., Jeon, S., Son, S., Chang, H., Yoon, H.I., Cho, Y.W., Swierczewska, M., Lee, S., Pomper, M.G., Kwon, I.C., Kim, K., Park, J.H., 2016. ROS-generating TiO2 nanoparticles for non-invasive sonodynamic therapy of cancer. Sci. Rep. 6.
Yumita, N., Nishigaki, R., Umemura, K., Umemura, S., 1989. Hematoporphyrin as a sensitizer of cell-damaging effect of ultrasound. Jpn. J. Cancer Res. 80, 219–222.
Yumita, N., Okudaira, K., Momose, Y., Umemura, S., 2010. Sonodynamically induced apoptosis and active oxygen generation by gallium-porphyrin complex, ATX-70. Cancer Chemother. Pharm. 66, 1071–1078.
Yumita, N., Iwase, Y., Nishi, K., Komatsu, H., Takeda, K., Onodera, K., Fukai, T., Ikeda, T., Umemura, S., Okudaira, K., Momose, Y., 2012. Involvement of reactive oxygen species in sonodynamically induced apoptosis using a novel porphyrin derivative. Theranostics 2, 880–888.